CHEMISTRY
A EUROPEAN JOURNAL

DOI: 10.1002/chem.200902101

# Evolution of Surface Morphology with Introduction of Stacking Faults in Zeolites

Neena S. John,[a] Sam M. Stevens,[a, b] Osamu Terasaki,[b] and Michael W. Anderson*[a]

**Abstract:** This paper sets out to try to determine some of the nanoscopic details of template action in zeolites. The problem has been addressed by monitoring the effects of competitive templating using, in particular, atomic force microscopy and high-resolution scanning electron microscopy. Using these techniques, it is possible to determine the subtle crystal growth changes that occur as a result of altering the concentration of these competitive templating agents. This work concerns the two important intergrowth systems MFI–MEL and FAU–EMT. It was found that some organic templating agents provide much greater structure-directing specificity. So much so in the case of the MFI–MEL system that a 2 mol % doping with the highly specific tetrapropylammonium cation drastically changes the fundamental growth processes. Furthermore, the effect of template crowding is shown to reduce specificity. This work shows how extensive frustrated intergrowth structures can still be accommodated within a nominal zeolite single crystal.

**Keywords:** crystal growth · scanning probe microscopy · structure-directing agents · surface analysis · zeolites

## Introduction

Zeolites constitute an important class of nanoporous materials that are widely used in industry as catalysts, molecular sieves and detergents.[1,2] There has been considerable interest in the scientific world to generate a variety of these porous structures in order to diversify their applications.[3–5] The crystal structure and, consequently, the crystal's utility, is heavily dependent upon a multitude of synthesis parameters such as temperature, gel precursors, aging, pH, organic templates and so forth. In the past few decades, there has been a greater thrust to understand the crystal growth mechanism in zeolites in order to have control of their properties.[5–7] Optical microscopy and X-ray scattering techniques have been employed initially to understand the kinetics of crystal growth from clear solutions.[8,9] Observing the internal and surface structure of the exposed faces of crystals synthesised under various conditions provide an alternative route to understand growth mechanisms in these materials. This demands nanometer resolution techniques and, hence, high-resolution scanning electron microscopy (HRSEM), high-resolution transmission electron microscopy (HRTEM) and atomic force microscopy (AFM) have been employed in recent years.[10–13] AFM is particularly advantageous in that it can be used either to look at crystal surfaces following synthesis (ex-situ) or in solution during growth (in-situ). AFM investigations of natural zeolites[14–16] and synthetic zeolites such as zeolite A,[17,18] silicalite-1,[19,20] zeolite Y[21] and zeolite L[22] have indicated a layer-by-layer growth mechanism, in which the particles add to the terrace edges, forming kinks followed by expansion of the terrace and simultaneous surface nucleation. The surface structure of silicalite-1 prepared using two different templates, that is, the tetrapropylammonium ion (TPA) and trimeric TPA, have also been elucidated by employing HRTEM and AFM techniques.[11] Quantification of layer heights by AFM has shown that they usually correspond to an identifiable structural unit of the zeolite which are the more stable structures.

There have also been numerous efforts to understand the growth in disordered intergrowth zeolites.[23–26] Intergrowths and defects arising due to stacking faults are of great importance as they can modify the pore dimensions and connectivity and have a large impact on applications. MFI–MEL and FAU–EMT are interesting systems for the investigation

[a] Dr. N. S. John, S. M. Stevens, Prof. M. W. Anderson
Centre for Nanoporous Materials, School of Chemistry
The University of Manchester, Manchester, M13 9PL (UK)
Fax: (+44) 161-275 4598
E-mail: m.anderson@manchester.ac.uk

[b] S. M. Stevens, Prof. O. Terasaki
Structural Chemistry, Arrhenius Laboratory
Stockholm University, 10691 Stockholm (Sweden)

Supporting information for this article is available on the WWW under http://dx.doi.org/10.1002/chem.200902101.

of stacking faults because they are related to the ZSM-5 and zeolite Y systems, respectively, which form the core catalysts of the petroleum industry. MFI and MEL belong to the pentasil family of zeolites and differ in the stacking of pentasil chains. In the [100] direction, the chains are related by inversion symmetry in MFI, and in MEL they are related by mirror symmetry. In the [010] direction, they are related by mirror symmetry in both MFI and MEL. This is reflected in the pore connectivity, as well as the size and morphology of the crystals. MFI has two types of channels, sinusoidal in the [100] direction and straight in the [010] direction, and MEL has straight channels in both directions.[27] Since MFI is the preferred product of usual synthetic routes, specific structure-directing agents (SDAs) are required for the synthesis of other pure polymorphs. The tetrapropylammonium ion (TPA) is highly specific for MFI and the terabutylammonium ion (TBA) is specific for MEL. The structural details are given in Figure 1.

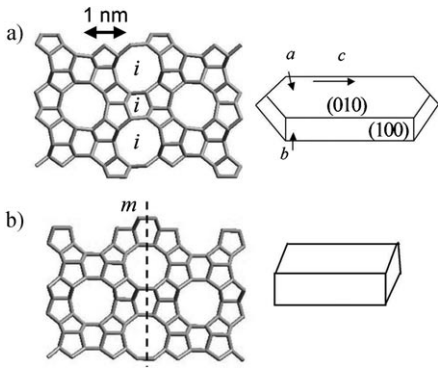


Figure 1. a) MFI and b) MEL framework structures viewed along (010) elucidating the inversion and mirror symmetry relation during stacking of pentasil chains. The constituent pentasil chain has a thickness of 1 nm. Sketches of preferred morphologies of MFI and MEL are also shown alongside.

FAU and EMT (Figure 2) both consist of sodalite cages connected by hexagonal prisms. In FAU, they connect in a manner to form an inversion point at the centre of the cage, and in EMT a mirror plane exists. FAU has a cubic unit cell, and EMT has a hexagonal unit cell with the sodalite cages connected in a wurtzite and zincblende arrangement, respectively. Specific SDAs such as [18]crown-6 (18C6) and [15]crown-5 (15C5) are used to synthesise the pure forms of EMT and FAU, respectively. By using a mixture of SDAs specific for each system in the synthesis gel (MFI–MEL[23,28–30] and FAU–EMT[31–33]), it is possible to vary the amount of intergrowths by varying the SDA compositional ratios. Such studies also help to develop an understanding of the role of organic templates in the crystal growth of zeolites.[34] The actual incorporation of TPA and TBA in MFI–MEL for TS-1 and TS-2 (titanosilicalites) has been studied by solid-state NMR spectroscopy.[29] Catalytic cracking efficiency of the pure and the faulted MFI and MEL has also been compared.[35] HRTEM studies have provided useful in-

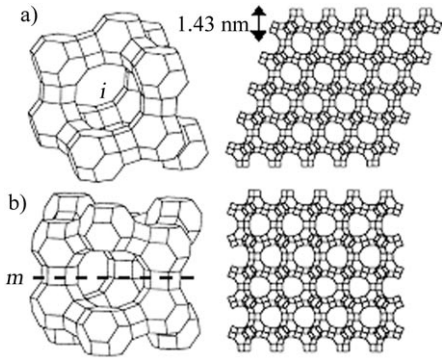


Figure 2. a) FAU and b) EMT framework structures illustrating the inversion and mirror symmetry relationship of the constituent faujasite sheets of thickness 1.43 nm. Two dimensional stacking patterns along [110] for FAU and $[100]_h$ for EMT are also shown.

sights into the internal structure of MFI–MEL faults in ZSM-5[28,36,37] and boron–MEL[38] and also FAU–EMT faults in zeolite Y.[32,40,41] There have been only a few attempts in the literature to study the surface structure of faulted crystals. The incorporation of faults should definitely affect the manner in which the growth units are added and hence will be reflected on the surface morphology of the crystals.

In this report, we present a combined AFM and HRSEM study of the surface morphology of the MFI–MEL intergrowths in silicalite, in which stacking faults are deliberately incorporated utilizing a co-templating method. In the earlier studies of surface structure of intergrowths using high-resolution microscopy,[33] the overall morphology of the pure members were not well defined and highly corrugated surfaces were observed in faulted as well as pure polymorphs. Hence, a clear understanding of the growth in MFI–MEL system has not been attained. We have investigated the morphology and surface topography of the entire compositional range of TPA and TBA in the synthesis gel. Co-templating using a more specific template for MEL, that is, the *N*-diethyl-3,5-dimethyl piperidinium ion, has also been studied. The utility of AFM has been extended to study the surface structure of FAU–EMT faults in high silica zeolite Y as well.

## Results and Discussion

The XRD patterns for silicalites MFI and MEL and the intergrowth samples prepared from TPA and TBA template mixtures are given in Figure 3a. P-100 (refer to experimental section for sample naming) shows characteristic reflections of MFI with an orthorhombic unit cell; however, in B-100, the number of reflections is less as expected for the more symmetric tetragonal unit cell in MEL.[25,42] In fact, we found that MEL prepared with 100% TBAOH has almost no extended MFI stacking faults as indicated by XRD. A 2% substitution of TBAOH by TPAOH (PB-2/98) in the synthesis mixture gives rise to a split in the reflections at $2\theta = 9°$ and 24°, and also other new reflections characteristic of MFI, indicating the presence of *i*-type stacking faults in-

  

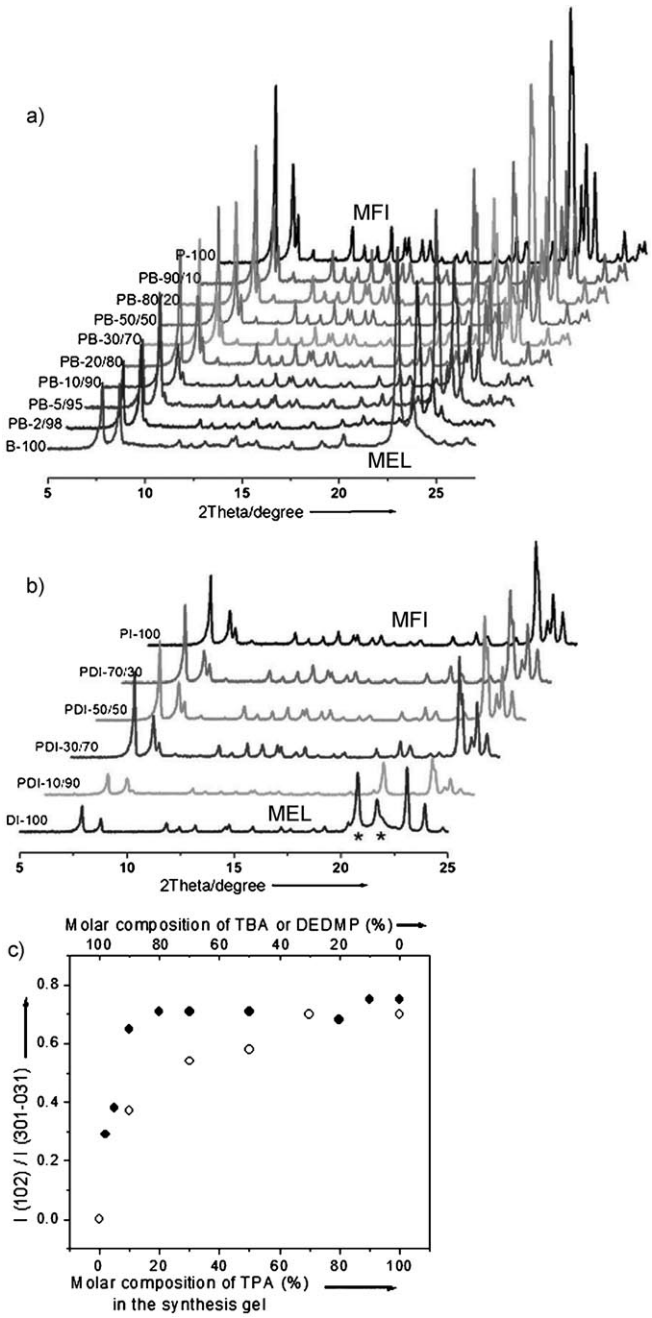


Figure 3. X-ray diffraction patterns for siliceous MFI–MEL zeolites with varying compositions of structure-directing agents in the synthesis gel, a) TPA and TBA and b) TPA and DEDMP, the asterisks represent peaks due to impure crystallographic phases. c) The calculated extended MFI stacking fault from XRD for various mixed compositions of templates; filled circles: TPA and TBA; hollow circles: TPA and DEDMP.

terrupting the σ-type stacking in MEL. With further addition of TPAOH, these reflections are seen to gain intensity similar to the MFI pattern. An estimation of the MFI intergrowth can be obtained from the ratio of the intensity of the (102) reflection ($2\theta = 14°$) to that of (301–031) multiplet ($2\theta = 15°$)[25,29] and is plotted against the template composition present in the synthesis mixture as shown in Figure 3c. In the case of 100% TBA, the (102) reflection is absent, indicating a pure MEL structure (see Supporting Information for a magnified view of the indicated peaks). However, powder XRD can give information only about extended stacking faults. There is a probability for local faults, which has been studied earlier using electron microscopy probes.[23,39] When a very small amount of TPAOH (2, 5 and 10%) is substituted for TBAOH, but still with excess of TBAOH in the mixture, it is possible to control the MFI intergrowth; however, when >20% TBAOH is substituted by TPAOH, the system becomes mostly MFI with fewer MEL stacking faults. This is similar to the observation by Tuel et al., in which the stacking fault probability was found to decrease drastically when more TBAOH is replaced by TPAOH for titanosilicalites.[29]

Since TBA is considered to be a weak templating agent for MEL, especially in the presence of TPA, we have studied the intergrowth probability using a piperidinium ion (DEDMP) template, a strong SDA for MEL[43,44] and TPA. Figure 3b gives the powder XRD patterns for the pure members and intergrowth silicalites, and a quantification of the MFI intergrowth occurrence with molar composition of the templates obtained from Figure 3b is plotted in Figure 3c. MFI–MEL intergrowth is more controllable than in the case of the TPA–TBA system. Stacking faults are present to a substantial extent even when 50% DEDMP is substituted by TPA, above which TPA takes over and the structure resembles MFI. With 100% DEDMP (DI-100), we observed the presence of minor extra crystallographic phases along with MEL, mainly quartz, marked with asterisks in Figure 3b. The impurity peaks are found to disappear as the amount of TPA increases in the synthesis mixture, indicating a complete conversion of silica to MFI silicalite. This again shows that TPA still strongly directs the structure, giving MFI as the preferred product.

Templates generally occupy the channel intersections or cages and participate from the nucleation stage of a zeolite, directing its final structure. The amount of SDAs that have actually gone into the product silicalite is best investigated by solid-state CP/MAS NMR spectroscopy of $^{13}C$ nuclei. Figures 4a and b give the $^{13}C$ NMR spectra of the silicalites incorporated with the templates TPA, TBA and DEDMP. The position and conformation of the templates within the MFI and MEL structures is in accordance with the reported trend.[29,45] The interesting observation here is the variation of the peak intensities of the carbons belonging to TPA and that of TBA in the intergrowth silicalites compared with the actual molar compositional ratio of the templates added during the synthesis. In Figure 4a, for the sample PB-2/98, a 2% substitution by TPAOH shows up as a splitting of the C4 (the farthest carbon from the nitrogen) position of TBA around 13 ppm and becomes stronger as the amount of TPAOH increases. The peaks in the region 10–20 ppm attain a complex appearance for samples PB-10/90 and PB-20/80, not only due to the superposition of peaks from TPA and TBA, but also possibly resulting from the interaction between adjacent TPAs and TBAs occluded in the channels. In

  

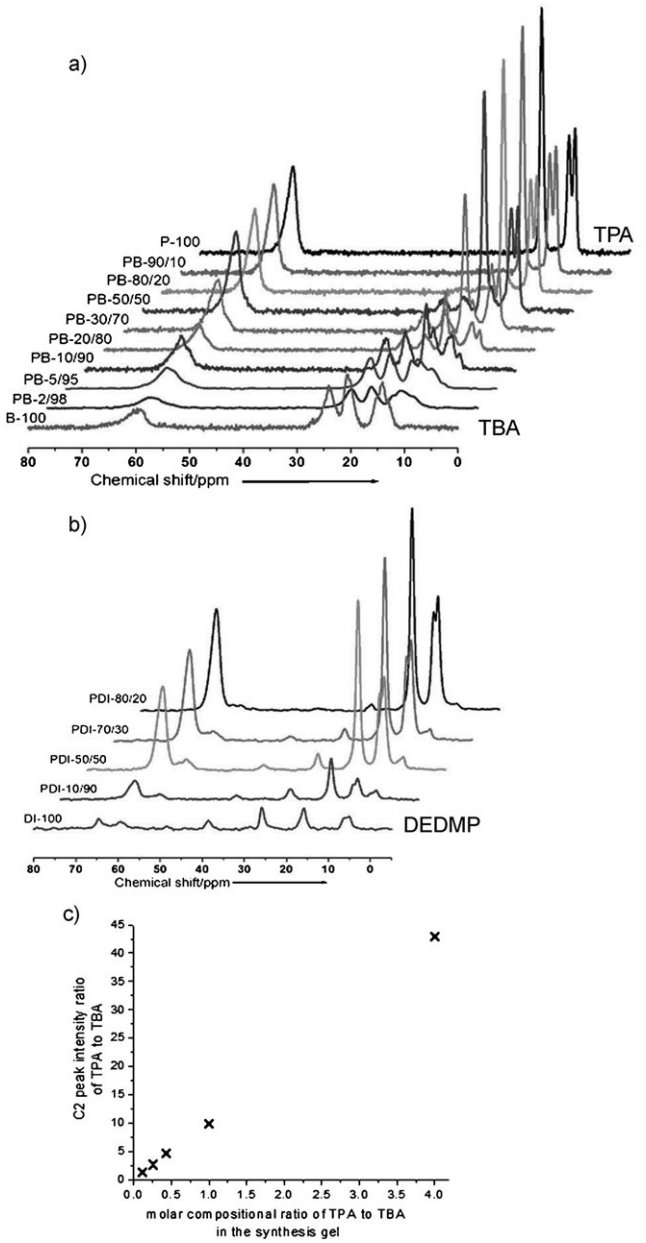


Figure 4. $^{13}$C CP/MAS-NMR spectra of siliceous MFI–MEL zeolites with varying compositions of structure-directing agents in the synthesis gel, a) TPA and TBA and b) TPA and DEDMP. c) A plot of the ratio of the intensities of C2 of TPA to that of TBA occluded in the crystal obtained from NMR against the ratio of percentage molar compositions of TPA to TBA in the synthesis gel.

the case of PB-50/50, it is easily discernible from the spectra that the ratio of TPA to TBA in the product silicalite is much higher than that in the synthesis gel. This is the case observed for other samples as well (Figure 4c), in which the ratio of the intensities of C2 (2$^{nd}$ carbon from nitrogen) of TPA to that of TBA calculated from Figure 4a is plotted against the ratio of molar percentage composition of TPA to that of TBA in the synthesis gel. However, it has to be taken under consideration that although four TPA cations can occupy one unit cell of MFI, only 2.6 cations occupy one MEL unit cell.[45] Molecular dynamic simulations have shown that due to steric hindrance from longer butyl chains, TBA occupies alternate channel intersections, and the smaller TPA fits perfectly inside the intersections, allowing them to occupy adjacent intersections.[46] Even when the above factor is considered, the TPA peaks are still intense. Finally, when there is a large excess of TPAOH in the gel, with only 10–20% substituted by TBAOH (PB-80/20 and PB-90/10), the product crystals contain negligible amounts of TBA. These results indicate that TPAOH is preferentially occluded, directing MFI structure particularly when more than 20% of TBAOH is replaced by TPAOH. This accounts for the extended MFI intergrowth seen in the XRD and, hence, a lower stacking fault probability for mixtures containing $>20$% TPAOH.

In contrast to TBA, DEDMP is a smaller template and can occupy all the channel intersections of MEL. Molecular dynamic studies showed that this is more energetically favourable for MEL than MFI and is, therefore, a powerful MEL directing template.[47] In Figure 4b, it can be seen that TPA peaks start showing up with 10% substitution of DEDMPI by TPAI (PDI-10/90) and gain strength as the TPA concentration in the gel increases, similar to the case of TPA–TBA. It is noticeable that the DEDMP peaks appear (PDI-80/20) even when only 20% DEDMP is present in the synthesis gel, indicating that DEDMP provides more competition to TPA than TBA. Hence, it is possible to get large stacking fault probabilities for a range of compositional ratios as seen in the XRD. Nevertheless, from the PDI-50/50 sample onwards, in which the TPA amount is greater, the TPA peaks are stronger than DEDMP peaks indicating that TPA is preferred when it is present in excess.

The growth of MFI–MEL intergrowth crystals were studied and compared with the pure polymorphs employing a combination of HRSEM and AFM. For this purpose, we have chosen a preparation method that gives a well-defined morphology and good facets for the pure silicalite-1 and silicalite-2 crystals such that any variation in the morphology and surface topography induced by the defects can be properly mapped. SEM and AFM images of the pure MFI and MEL end-members are given in Figure 5. The low-magnification SEM image of silicalite-1 (Figure 5a) shows that the majority of the crystals have a rounded, boat-shape morphology with dimensions of roughly $11\times5\times15$ μm ($a\times b\times c$). Some crystals have complex shapes arising from 90° growths and at other angles which is a common phenomenon seen with most preparations of silicalite-1.[48] Although MFI can have several types of local nanoscale defects,[23,38,49] we focused on extended defects giving rise to closely related MEL structures. Hence, for crystal growth investigations of MFI–MEL intergrowths, we selected crystals with uniform shapes under the microscope. The AFM image of the flat (010) facet of the silicalite-1 given in Figure 5b reveals nanometer details of the surface consisting of concentric layers forming terraces and steps, following the boundaries of the whole crystal itself generating its final morphology. A cross-section analysis of the layers gives the step-height

  

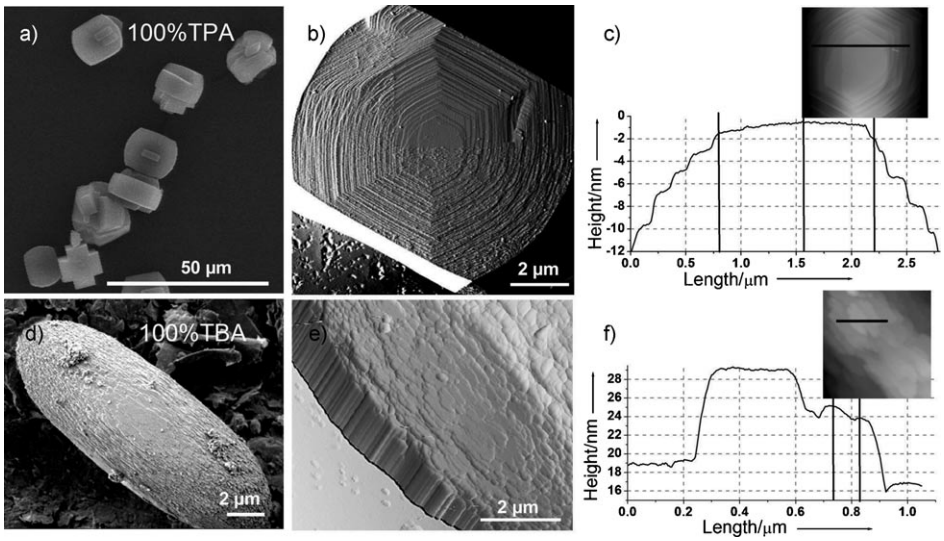


Figure 5. a), b) SEM and deflection AFM images of (010) facet of silicalite-1 (MFI) with 100% TPA (sample: P-100), respectively. c) Cross-section analysis of b) across the line in the height image as shown in the inset. d), e) HRSEM and AFM images of (010) facet of silicalite-2 (MEL) with 100% TBA (sample:B-100), respectively. f) Cross-section analysis of e) across the line as shown in the inset. Solid vertical lines denote the measurement of 1 nm heights.

values to be about 1 nm (see Figure 5c), which can be related to the thickness of a pentasil chain, the periodic building unit of MFI (see Figure 1). Step height values of integer numbers of unit cells (2, 3 etc.) are also often observed where two or three terraces merge. Hence, the crystals grow by a layer-by-layer mechanism[50] such that after the formation of stable nuclei, pentasil chains stack in the required symmetry of MFI, directed by the adsorbed template during its growth. Such layer-by-layer growth of pentasil sheets has been observed in other preparations of silicalite.[19,20] In the present case, we also observed the directional nature in the layers itself with slower growth in the [001] direction, resulting in an elongated *c* dimension. The other pure end member of the intergrowth series, MEL silicalite-2, formed ovate-shaped crystals of dimensions of about. $5\times15$ μm ($a=b\times c$), when prepared under identical conditions as silicalite-1 (except the replacement of TPA by TBA) as shown in Figure 5d. The crystal shape is closely related to the expected tetragonal morphology. HRSEM and AFM images (Figure 5d and e, respectively) indicate a layer growth in this case as well, but the layers are irregularly shaped due to a high density of kink sites. Most of the terraces possess short widths with step-heights as large as 10 nm (Figure 5f). The smallest value for a step-height is 1 nm corresponding to the pentasil chain thickness. The presence of kink sites and higher step-heights implies a random surface nucleation, in which several two-dimensional nuclei form on the surface at a time, which then spreads outwardly and coalesce with other spreading terraces. Locally generated MFI defects might also cause such growth patterns. HRSEM images are useful in this case because they give a clearer picture of the curved facets and sides of the crystals. In AFM they are often susceptible to artifacts from tip convolution effects.[51]

Figure 6 shows HRSEM and AFM images of MFI–MEL intergrowth crystals prepared using a binary mixture of templates, TPA and TBA in various molar compositional ratios (PB sample series). When 2 or 5% of TBAOH is substituted by TPAOH, the crystals are still ovate; however, a major change in the morphology is seen with respect to the dimensions along *a*, *b* and *c* axes which, become non-equivalent (Figures 6a and c). The average sizes are about $6\times5\times20$ μm and $8\times5.5\times20$ μm, respectively, for samples PB-2/98 and PB-5/95. Distinct (010) and (100) facets begin to appear, influenced by the presence of MFI intergrowths directed by the TPA template. This is also supported by XRD results. An examination of the surface topography by HRSEM (Figures 6b and d) reveals the presence of thicker layers (20–25 nm) protruding from the curved edges composed of terraces of smaller widths. With 10% substitution of TBAOH by TPAOH (PB-10/90), there is a drastic change in the morphology, which is now a rounded brick-shape with a size of about $5.5\times2.5\times11$ μm as shown in Figure 6e. HRSEM and AFM images in Figures 6f and g, respectively, show the surface of the crystals to be covered with block-like features protruding about 50–150 nm above the surface, as gathered from the cross-section data (Figure 6h). Each block feature consists of smaller terraces of 1 nm or multiple step-heights. Both (010) and (100) facets have similar topography as seen from HRSEM, consisting of thicker layers projecting as needle-shaped blocks (100 nm) towards the edges. The overall morphology of the crystals, with a size of about $9\times5\times17$ μm, starts resembling the pure MFI morphology when a further 10% TPAOH is added (PB-20/80). Block-like features are again seen on the (010) facet of the crystal with a height of 25–100 nm (Figures 6i, j and k) from the surface, and the (100) facet seems to be unaffected, bearing characteristic rectangular terraces following the shape of the facet. With further replacement of TBAOH by TPAOH, for example for samples PB-30/70, PB-50/50 and PB-80/20 (Figures 6l–s), the crystals appear more or less like MFI crystals (P-100, Figure 5a) in SEM images. A high-resolution SEM (Figure 6l) and AFM scanning reveal that the (010) surface has concentric circular terrace patterns, sometimes with more than one nucleation centre (Figures 6l–s). The circular terraces have ragged edges giving the appearance of flowery patterns. This is caused by the presence of a high density of kink sites. Towards the centre of origin of the terrace pattern, the step heights are 1 nm or multiples thereof. However, towards the

  

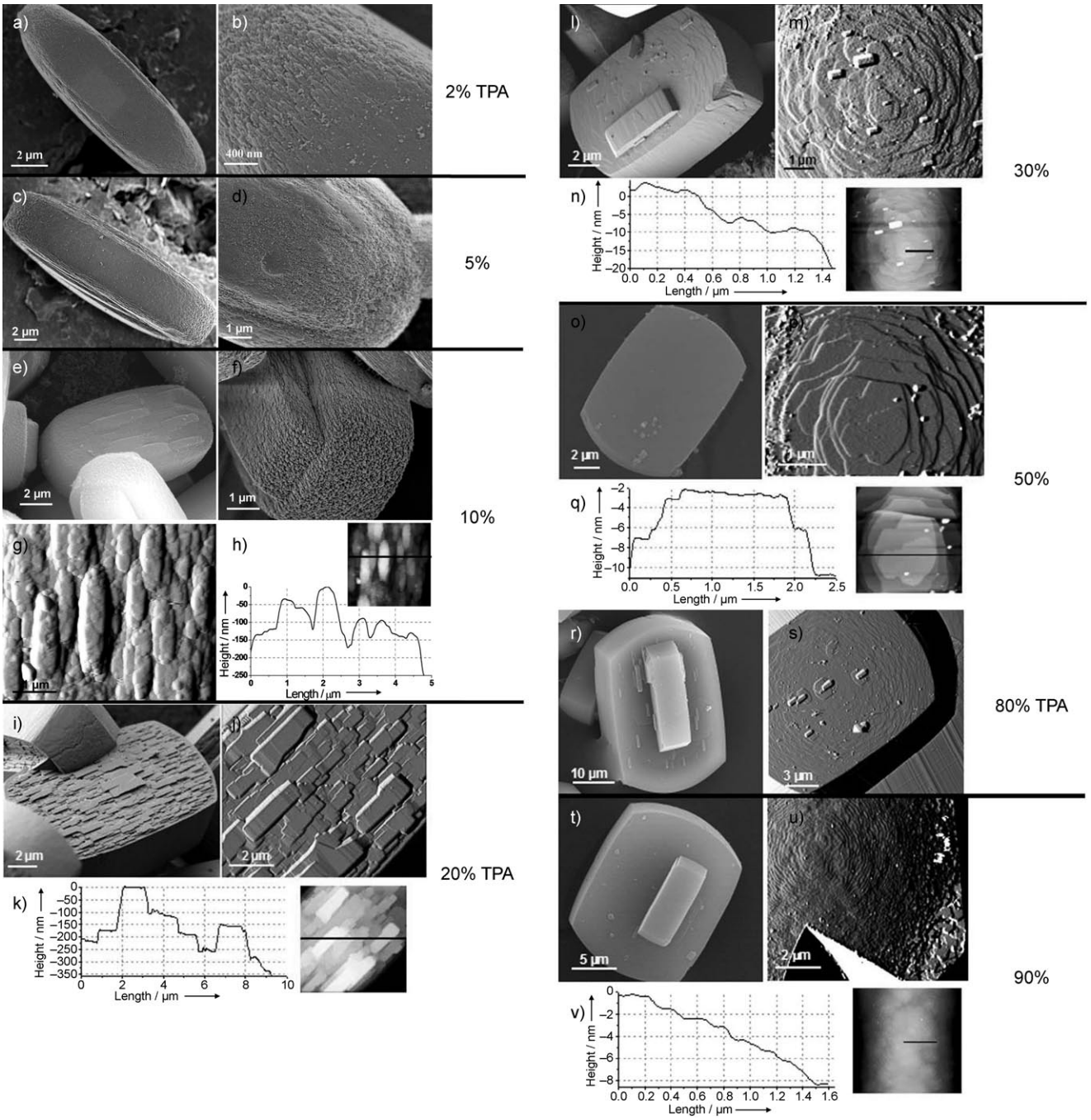


Figure 6. HRSEM and deflection AFM images showing the (010) facet of MFI–MEL obtained with various compositional ratios of TPA and TBA in the synthesis gel. a), b) 2% TPA:98% TBA; HRSEM images. c), d) 5% TPA:95% TBA; HRSEM images. e) 10% TPA:90% TBA; HRSEM image. f) A closer look at e) showing the block growth. g) Deflection AFM image of e). h) Cross-section analysis of e) across the black line as shown in the height image alongside. i), j) 20% TPA:80% TBA; HRSEM and AFM images, respectively. k) Cross-section analysis of j) along the line in the height image alongside. l), m) 30% TPA:70% TBA; HRSEM and AFM images, respectively. n) Cross-section analysis of m) along the line in the height image shown alongside. o), p) 50% TPA:50% TBA; SEM and AFM images, respectively. q) Cross-section data. r), s) 80% TPA:20% TBA; SEM and AFM images, respectively. t), u) 90% TPA:10% TBA; SEM and AFM images, respectively. v) Cross-section data along the line in the height image shown alongside.

edges of the crystals, the terraces merge and higher step heights of 10 nm are also observed. When only 10% TBAOH is present with an excess of TPAOH, very subtle changes on the surface morphology are seen. The directional nature of the terraces seen in P-100 crystals disappears and the terraces become circular in PB-90/10 (Figure 6u). A typical step trace given in Figure 6v gives the height values to be 1 nm. In Figure 6u, it is noticeable that beneath the growth, towards the edges of the crystal, terraces of large step heights (6–8 nm) appear.

  

When the TPAOH concentration in the gel is low ($\leq$ 20%) compared to that of TBAOH, extended MFI stacking faults interrupt the MEL growth that appear as blocks or thicker layers on the (010) surface. Agger et al. have observed this phenomenon in MFI crystals during some of their preparations.[19] When the pentasil chains stack on the surface of a MEL nucleus, there is a high probability for the chains to attach to the surface with inversion symmetry rather than mirror symmetry expected for the MEL structure. This in turn causes unsatisfied Si–O bonds as the pentasil chains are unable to connect to the rest of the framework in the other direction. Consequently, back-to-back defects and double defects are formed in the system.[19] The next addition of a pentasil chain will have a higher tendency to connect with inversion symmetry and hence an MFI nucleus is formed. The formation of such nuclei interrupts the smooth growth and manifests as thicker layers and blocks on the surface (see Supporting Information). The probability for the formation of MFI nuclei will depend on the directing power of the template TPA, and, in the present case, our NMR studies have shown that when TPAOH is low with excess of TBAOH, the entire amount of TPA added goes into the crystal. This is further supported by $^{13}C$ analysis of the supernatant solution after the formation of the product, which showed only peaks for TBAOH, even for the sample PB-20/80, implying TPAOH is a powerful SDA. TPA becomes the dominant template at higher TPA compositions (>20%), and the system has predominantly *i*-type stacking. This is manifested in the shape of the crystals; they become more MFI-like. However, the surface is seen to be highly sensitive to the presence of intergrowths. The stacking faults decrease with increase in TPA concentration, and, hence, the intergrowth protrusions on the (010) facet disappear and the surface becomes smooth. However, signatures of interruptions in normal crystal growth are seen as ragged edges of the circular terraces. The presence of a high density of kink sites might arise from the slowing down of the terrace spread wherever MEL nucleates directed by TBA. These subtle changes are caused by the incorporation of a small amount of TBA, giving rise to local defects not detectable from XRD or normal SEM images.

Figure 7 shows the SEM and AFM images of MFI–MEL intergrowths prepared from co-templating of TPA and DEDMP. With 100% DEDMP, perfectly tetragonal shaped MEL crystals are obtained (Figure 7a). A layer-by-layer growth is observed from surface topography, consisting of 1 nm high concentric circular terraces spreading towards the edges revealed by the AFM image and its cross-sectional analysis in Figures 7b and c. With 10% substitution of DEDMP by TPA, a drastic change in morphology is seen as in the case of TPA and TBA, but the morphology is different exhibiting a cuboid shape in this case (Figure 7d). Terasaki and co-workers also observed a similar morphology in B–MEL when boron was introduced in the synthesis gel of MEL with DEDMP template.[38] HRTEM studies have indicated MFI stacking faults in B–MEL crystals. Our surface analysis by AFM of PDI-10/90 shows protruding layers of

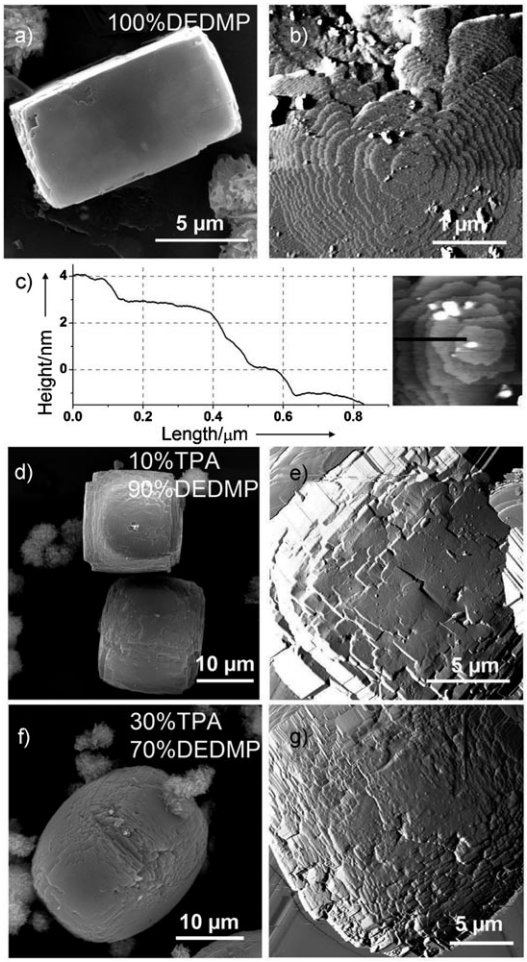


Figure 7. SEM and deflection AFM images of MEL and MFI–MEL with various molar compositional ratios of TPA and DEDMP in the synthesis gel. a), b) 100% DEDMP; SEM and deflection AFM images, respectively. c) Cross-section analysis of b) along the line given in the inset height image. d), e) 10%TPA:90%DEDMP; SEM and deflection AFM images, respectively. f), g) 30%TPA:70%DEDMP; SEM and deflection AFM images, respectively.

large heights implying interrupted growth (Figure 7e). A similar growth mechanism resulting from the formation of MFI and MEL nuclei as in the case of the TPA–TBA system can be proposed here. With 30% replacement of DEDMP by TPA (PDI-30/70), the morphology again changes drastically to be more like MFI as seen from the SEM image in Figure 7f. Surface morphology shows a block type growth, similar to the case of PB-10/90 and PB-20/80 with a significant amount of MFI–MEL intergrowths (Figure 7g). The intergrowth faults are still present to a good extent in TPA-DEDMP system; however, for the TPA–TBA system, they decrease as the TPA concentration increases to more then 20% in the synthesis gel. It is also noticeable that the amount of intergrowth faults formed is approximately proportional to the molar ratio of the template that is occluded in the crystals, although it is not the absolute ratio initially added in the synthesis gel (see XRD and $^{13}C$ NMR spectra in Figures 3 and 4). A closer competition

  

provided by DEDMP to TPA than TBA can be attributed to its smaller size enabling it to occupy every channel intersection as in the case of TPA; TBA is sterically hindered. The amount of specific template taken up during nucleation and crystal growth directs the stacking of pentasil units to form MFI or MEL, which is also reflected in the surface morphology.

We have also investigated the influence of FAU–EMT intergrowths on the surface morphology of zeolite Y. Figure 8 shows the XRD patterns of zeolite Y samples obtained with

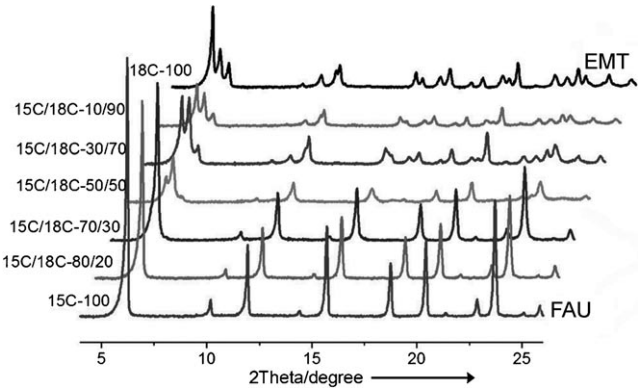


Figure 8. X-ray diffraction patterns showing the systematic variation of FAU–EMT stacking faults in zeolite Y obtained by varying compositional ratios of structure-directing agents, 15C5 and 18C6.

various molar compositional ratios of SDAs 15C5 (FAU directing) and 18C6 (EMT directing). The reflections in the $2\theta$ range 5–7° are distinctive for FAU or EMT structure. FAU has only the (111) reflection (sample 15C-100) while EMT has $(110)_h$, $(002)_h$ and $(101)_h$ reflections (sample 18C-100) in this region. When 30% 15C5 is substituted by 18C6 in the synthesis gel, the product (15C/18C-70/30) does not contain extended EMT faults. However, EMT reflections start emerging in the XRD pattern when 15C5 and 18C6 are present in equal molar ratios (sample 15C/18C-50/50), indicating the formation of FAU–EMT intergrowths. Above 50% 18C6 in the synthesis gel, EMT reflections gain strength. This is in agreement with the previous intergrowth studies under static conditions.[31–33] It is challenging to understand the intergrowth formation from XRD, as the information is limited to faults of long-range order. Hanif et al.[52] have shown that stirring during the synthesis can avoid transport-limited diffusion, constantly exposing the growing crystal surface to template molecules. They found that under such conditions 18C6 is the preferential template and intergrowth formation is reduced to a narrow range of crown ether compositions. We have looked at the detailed surface morphology of pure end-members and intergrowths prepared under static conditions. Figure 9 shows the SEM and AFM images of pure phase FAU and EMT. FAU forms octahedral crystals exposing the (111) facet following a layer-by-layer growth mechanism (see Figures 9a and b). The layers bear the ternary symmetry of the (111) facet but

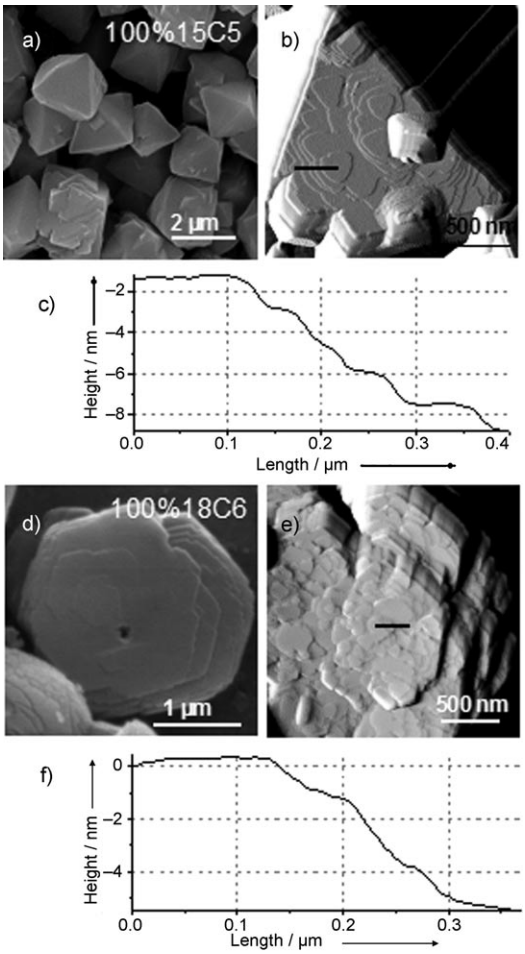


Figure 9. SEM and deflection AFM images of zeolite Y. a), b) (111) facet of FAU with 100% 15C5, respectively. c) Cross-section analysis showing a typical step train across the black line in b). d), e) (001) facet of EMT with 100% 18C6; SEM and AFM images, respectively. f) Cross-section analysis along the line in e).

are seen rotated 60° with respect to the facet. Multiple nucleation sites are also seen. A typical step trace on the surface is shown in Figure 9c and the steps are 1.45–1.5 nm high corresponding to the thickness of a faujasite sheet (see Figure 2), as established previously for zeolite Y.[21] A few crystals revealed growths due to spiral growth (see Supporting Information). Layers of 1.43 nm are also observed on hexagonal platelets of EMT with two-dimensional multiple nucleation sites (Figures 9d–f).

The SEM and AFM images of various FAU–EMT intergrowth members are shown in Figure 10. With 10% substitution of 18C6 by 15C5 in the precursor gel, the crystals resemble pure EMT (Figure 10a), but the AFM image in Figure 10b clearly shows small particulates on the hexagonal facet. When the 15C5 concentration is increased to 30%, the particulates develop to form smaller isolated octahedral crystals (Figures 10c and d). The surfaces of these overgrown crystals have triangular terraces similar to the (111) facet of FAU (Figure 10d). With 50% substitution of 18C6 by 15C5, there is a merged growth of octahedral crystals of

  

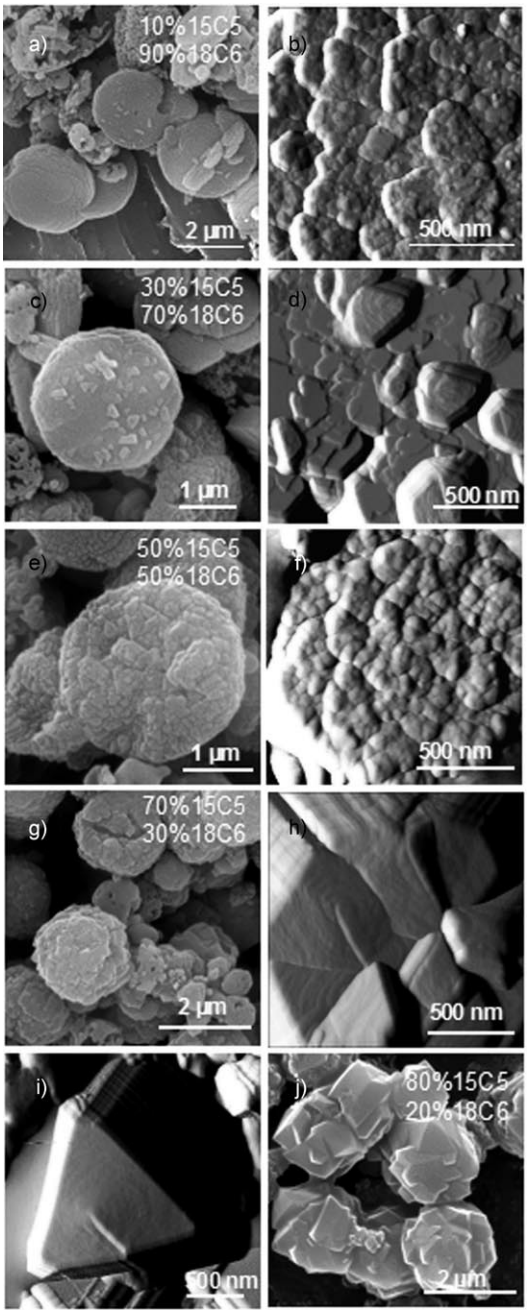


Figure 10. SEM and AFM deflection images showing the morphology of FAU–EMT obtained with various compositional ratios of SDAs 15C5 and 18C6 in the synthesis gel. a), b) 10%15C5:90%18C6, respectively. c), d) 30%15C5:70%18C6, respectively. e), f) 50%15C5:50%18C6, respectively. g), h) 70%15C5:30%18C6, respectively. i) 70%15C5:30%18C6, AFM image showing a dislocation on (111) where twinning arises. j) 80%15C5:20%18C6; SEM image.

FAU and hexagonal platelets of EMT generating a rougher surface as seen in Figures 10e and f. Twinned crystals of FAU giving rise to a hexagonal morphology are seen when 70% of 15C5 is present in the synthesis gel (Figures 10g and h). Dislocations are observed on the surface of twinned crystals (Figures 10h and i). With excess of 15C5 (sample 15C/18C-80/20), FAU crystals with multiple twinning are formed (Figure 10j).

Clear evidence for FAU–EMT intergrowths is seen as the emergence of (111) facets of FAU on hexagonal plates of EMT, with 30% replacement of 18C6 by 15C5. As the concentration of 18C6 decreases in the synthesis gel, crowding of FAU octahedra are seen, but still an overall hexagonal morphology is retained. Although the FAU octahedra appear to be overgrown on EMT platelets similar to the case of epitaxial growth of FAU on EMT,[53] earlier TEM studies of the internal structure[52] have shown that they are actually intergrown crystals. As the XRD (Figure 8) also indicates, extended FAU and EMT stacking are present in these systems. With 70% or 80% 15C5 in the synthesis gel, multiple twins of FAU octahedra can generate local EMT structures.[54] Such local faults cannot contribute to the XRD. Treacy et al. have shown that segregated or random FAU and EMT stacking occurs in many zeolites through simulation studies.[40] Hence, under static conditions FAU–EMT intergrowths are obtained for a broad range of molar ratios of crown ethers, which is supported by previous TEM studies. However, a slight dominance of 18C6 is noticed in preserving a hexagonal morphology even at lower 18C6 concentrations. 18C6 is a better fit in the hypocage of EMT than in the supercage of FAU or EMT and hence more powerful than 15C5.[34] Under stirred conditions, 18C6 is the preferred template and intergrowths are observed only for a narrow range of crown ether molar ratios and, at lower 18C6 concentrations.[52]

## Conclusion

By performing competitive templating experiments in zeolites and studying the nanoscopic effect by atomic force microscopy and high-resolution scanning electron microscopy, we have elucidated some key steps in the structure directing behaviour. It was shown that when TPA is present as a dopant in the preparation of MFI–MEL intergrowth structures, it rapidly plays a dominant structure directing role over TBA. This is probably due to a combination of an enhanced keying of the TPA molecule to the crystal growth surface combined with the crowding of TBA molecules, which prevents adsorption at every channel intersection. As a consequence, TBA is a rather weak structure directing agent which, although it will produce pure MEL when used without competition, results in a crystal exhibiting a microcystalline nature owing to faulting. In the presence of the smaller DEDMP molecule, which can be accommodated at every intersection, not only is there a progressive change from MFI to MEL upon replacement of TPA, but also the MEL crystals show much less faulting. In mixed TPA–TBA preparations, in which there is an extensive degree of faulting and intergrowths, these are accommodated as small aligned crystallites. In the FAU–EMT systems the [18]crown-6 template plays the dominant templating role often incorporated preferentially over [15]crown-5 and re-

  

sults in an overgrowth of small FAU crystals on EMT only when the concentration of [18]crown-6 is depleted in solution.

## Experimental Section

**Synthesis of silicalite sample series**

*PB series*: Silicalite-1 (MFI) and silicalite-2 (MEL) were prepared following a previously reported method.[42] Tetrapropylammoniumhydroxide (TPAOH) and tetrabutylammoniumhydroxide (TBAOH) were used as SDAs for MFI and MEL, respectively. A mixture of the SDAs in various proportions was used to synthesise MFI–MEL intergrowth silicalites. The gel composition for the synthesis was $0.1\,SiO_2$:$0.012\,(x$TPAOH+$(1-x)$TBAOH):$0.04\,NH_3$:$1.1\,H_2O$, $x=1$, 0.9, 0.8, 0.5, 0.3, 0.2, 0.1, 0. Moist silicic acid (15% $SiO_2$, BDH, AR) was used as the silica source and 40% aqueous TPAOH and TBAOH (Aldrich) were used as SDA sources. SDAs were added to the silicic acid, de-ionised water and ammonia mixture taken in the required molar ratios and was stirred thoroughly for 4–5 h until a homogeneous, flowing gel was obtained. For intergrowth silicalites, a binary mixture of TPAOH and TBAOH in the required molar ratios was prepared and added to silicic acid, ammonia and water mixture followed by stirring. The mixture was then transferred to a Teflon-lined stainless steel autoclave and heated at 170 °C for 3 days. The autoclave was quenched in cold water after 3 days and the white crystalline product was filtered, washed with copious amounts of de-ionised water and dried at 90 °C in a normal aerated oven. Quenching and subsequent washing and sonication of crystals in water often helped in avoiding secondary nucleation of crystallites observed during slow cooling of the crystals in the autoclave and in removing adsorbed foreign particles, respectively, thus providing clean surfaces for examination under AFM. Except for the SDA type and molar ratio, the experimental conditions were maintained constant throughout the preparation of the sample series.

When $x=1$, for 100 mol% TPAOH in the gel, the resultant sample is named as P-100, and when $x=0$, 100 mol% TBAOH, the sample is named B-100. When $x=0.9$, 90 mol% TPAOH and 10 mol% TBAOH is present in the gel, the sample is named as PB-90/10. Similarly a series of samples, PB-80/20, PB-70/30, PB-50/50, PB-30/70, PB-20/80, PB-10/90, PB-5/95 and PB-2/98 were prepared. Hence, the sample name PB-5/95 indicates that 5 mol% of TPAOH and 95 mol% of TBAOH were used in the precursor gel.

***PDI series***: A series of silicalite samples with SDAs as tetrapropylammonium iodide (TPAI, MFI directing) and *N*,*N*-diethyl-3,5-dimethylpiperidinium iodide (DEDMPI, MEL directing) was also prepared. DEDMPI was prepared in the laboratory following a method by Nakagawa et al.[43] Silicalites were prepared from the gel composition, $10\,SiO_2$:$0.75\,(x$TPAI+$(1-x)$DEDMPI):$6\,KOH$:$600\,H_2O$, $x=1$, 0.7, 0.5, 0.3, 0.1, 0. LUDOX AS-40 colloidal silica was used as the silica source and KOH as the base. TPAI or DEDMPI or a binary mixture in the required molar ratio was dissolved with stirring in KOH and de-ionised water. Colloidal silica was then added to the above mixture and stirred for 24 h. The resulting clear solution was then transferred to a Teflon-lined stainless steel autoclave and heated at 170 °C for 3 days. The autoclave was quenched after the reaction, the white product filtered and washed with de-ionised water and dried at 90 °C. The samples are named in a similar manner as in the previous case and hence, PI-100 indicates the presence of 100 mol% TPAI, DI-100, 100 mol% DEDMPI and PDI-70/30, 70 mol% TPAI and 30 mol% DEDMPI in the precursor gel. The other samples prepared in the series are PDI-50/50, PDI-30/70 and PDI-10/90.

**Synthesis of zeolite Y sample series**: FAU and EMT zeolite Y were prepared using SDAs [15]crown-5 (15C5) and [18]crown-6 (18C6), respectively. A mixture of these SDAs in various proportions was used to synthesise FAU–EMT intergrowths. The molar composition of the gel was $10\,SiO_2$:$1\,Al_2O_3$:$1\,(x$15C5+$(1-x)$18C6):$2.4\,Na_2O$:$140\,H_2O$, $x=1$, 0.8, 0.7, 0.5, 0.3, 0.1, 0. LUDOX AS-40 colloidal silica (Aldrich) and sodium aluminate (48% $Na_2O$ and 52% $Al_2O_3$, Riedel-de Haën) were used as the silica and alumina source, respectively. Sodium aluminate was dissolved in NaOH and de-ionised water and added to the crown ether dissolved in water or a mixture of crown ethers in required ratio for intergrowth samples in a polypropylene bottle. Colloidal silica was added drop-wise to the above mixture resulting in a gel. The gel was then stirred for 24 h to make it homogeneous and aged for another two days at room temperature. The thickened gel was stirred again before transferring to a 95 °C oven and kept for 8 days. The reaction vessel was quenched in cold water and the white solid was filtered, washed with de-ionised water and dried at 70 °C for 24 h.

The samples are named as 15C-100, for 100 mol% 15C5 in the precursor gel ($x=1$) and 18C-100, for 100 mol% 18C6 in the gel ($x=0$). When $x=0.8$, the sample is named as 15C/18C-80/20, which denotes the presence of 80 mol% of 15C5 and 20 mol% of 18C6.The other samples prepared in the series are 15C/18C-70/30, 15C/18C-50/50, 15C/18C-30/70, 15C/18C-10/90.

**Characterisation of samples**: **XRD**: Powder XRD patterns were recorded on a Philips X′pert diffractometer using $Cu_{K\alpha}$ radiation (1.5418 Å). As-synthesised, dried samples were thoroughly ground to a fine powder before mounting in a stainless steel holder and were revolved at 16 Hz during acquisition. All scans were run between $2\theta$ values of 5 and 50°, at a continuous scan rate of $0.016°\,min^{-1}$.

**NMR spectroscopy**: Solid-state $^{13}C$ NMR spectra were acquired using Bruker Avance III 400. Samples were spun at 10 kHz in zirconia rotors and sampling rate was 1000. $^{13}C$ CP/MAS spectra were recorded using a cross-polarisation sequence with ramped contact pulse of 2 ms contact time, spinal-64 decoupling and 5 s repetition time. For quantification, the peaks were fitted using a 50:50 mixed Gaussian-Lorentzian equation employing Bruker TOPSPIN software.

**HRSEM**: SEM images were obtained using a FEI Quanta 200 instrument with field emission gun. Samples were prepared by spreading zeolite powder on a carbon tape stuck on a metal stub followed by sputter coating with gold to reduce charging effects under electron beam. For acquiring high-resolution SEM images, samples were placed on a conductive surface but left uncoated and were taken using a JEOL JSM-7401F (cold-FESEM) using the Everhart–Thornley secondary electron detector.

**AFM**: AFM was done in contact mode using commercial silicon nitride cantilevers on a JPK Nanowizard II instrument. The samples were prepared by drop casting an aqueous dispersion of zeolite powder onto a heated flattened piece of thermoplastic, which, when cooled, had crystals embedded with facets protruding out of the surface. The crystals are located under the optical microscope of the AFM and the cantilever is positioned over a facet for AFM scanning. The scan rate was normally 1 Hz. XY plane-fit and height analyses were performed using JPK image processing software.

## Acknowledgements

The authors are grateful to the EPSRC and ExxonMobil Research and Engineering for funding. Thanks are due to PakYan Moh and Dr. Patrick Hill for technical assistance with NMR and SEM measurements. The authors also thank Prof. Colin Cundy, Dr. Jonathan Agger, Dr. Francis Taulelle, Prof. Paul Wright and other members of the Nanogrowth team for useful discussions. The authors thank the Knut and Alice Wallenberg Foundation for support of the Electron Microscope Centre, Stockholm University.

[1] a) "Zeolites as Catalysts, Sorbents and Detergent Builders-Applications and Innovations": *Studies in Surface Science and Catalysis, Vol. 46* (Eds.: H. G. Karge, J. Weitkam), Elsevier, Amsterdam, **1989**, pp. 3–871; b) A. Corma, *Chem. Rev.* **1995**, *95*, 559–614.

[2] J. A. Rabo, M. W. Schoonover, *Appl. Catal. A* **2001**, 222, 261–275.

[3] R. M. Barrer, *Hydrothermal Chemistry of Zeolites*, Academic Press, London, **1982**.

[4] C. S. Cundy, P. A. Cox, *Chem. Rev.* **2003**, *103*, 663–701.

  

[5] C. S. Cundy, P. A. Cox, *Microporous Mesoporous Mater.* **2005**, 82, 1–78.
[6] S. Mintova, N. H. Olson, V. Valtchev, T. Bein, *Science* **1999**, *283*, 958–960.
[7] T. M. Davis, T. O. Drews, H. Ramanan, C. He, J. Dong, H. Schnablegger, M. A. Katsoulakis, E. Kokkoli, A. V. Mccormick, R. L. Penn, M. Tsapatsis, *Nat. Mater.* **2006**, 5, 400–408.
[8] C. S. Cundy, B. M. Lowe, D. M. Sinclair, *Faraday Discuss.* **1993**, *95*, 235–252.
[9] C. J. Y. Houssin, C. E. A. Kirschhock, P. C. M. M. Magusin, B. L. Mojet, P. J. Grobet, P. A. Jacobs, J. A. Martens, R. A. van Santen, *Phys. Chem. Chem. Phys.* **2003**, *5*, 3518–3524.
[10] O. Terasaki, T. Ohsuna, *Catal. Today* **1995**, *23*, 201–218.
[11] I. Díaz, E. Kokkoli, O. Terasaki, M. Tsapatsis, *Chem. Mater.* **2004**, *16*, 5226–5232.
[12] a) M. W. Anderson, T. Ohsuna, Y. Sakamoto, Z. Liu, A. Carlssond, O. Terasaki, *Chem. Commun.* **2004**, 907–916; b) M. W. Anderson, *Curr. Opin. Solid State Mater. Sci.* **2001**, *5*, 407–415.
[13] S. M. Stevens, P. Cubillas, K. Jansson, O. Terasaki, M. W. Anderson, P. A. Wright, M. Castro, *Chem. Commun.* **2008**, 3894–3896.
[14] A. L. Weisenhorn, J. E. MacDougall, S. A. C. Gould, S. D. Cox, W. S. Wise, J. Massie, P. Maivald, V. B. Elings, G. D. Stucky, P. K. Hansma, *Science* **1990**, *247*, 1330–1333.
[15] J. E. MacDougall, S. D. Cox, G. D. Stucky, A. L. Weisenhorn, P. K. Hansma, W. S. Wise, *Zeolites* **1991**, *11*, 429–433.
[16] S. Yamamoto, S. Sugiyama, O. Matsuoka, K. Kohmura, T. Honda, Y. Banno, H. J. Nozoye, *J. Phys. Chem.* **1996**, *100*, 18474–18482.
[17] J. R. Agger, N. Pervaiz, A. K. Cheetham, M. W. Anderson, *J. Am. Chem. Soc.* **1998**, *120*, 10754–10759.
[18] S. Dumrul, S. Bazzana, J. Warzywoda, R. R. Biederman, A. Sacco, Jr., *Micro. Meso. Mater.* **2002**, *54*, 79–88.
[19] J. R. Agger, N. Hanif, C. S. Cundy, A. P. Wade, S. Dennison, P. A. Rawlinson, M. W. Anderson, *J. Am. Chem. Soc.* **2003**, *125*, 830–839.
[20] L. I. Meza, M. W. Anderson, J. R. Agger, C. S. Cundy, C. B. Chong, R. J. Plaisted, *J. Am. Chem. Soc.* **2007**, *129*, 15192–15201.
[21] M. W. Anderson, J. R. Agger, J. T. Thornton, N. Forsyth, *Angew. Chem.* **1996**, *108*, 1301–1304; *Angew. Chem. Int. Ed. Engl.* **1996**, *35*, 1210–1213.
[22] R. Brent, M. W. Anderson, *Angew. Chem.* **2008**, *120*, 5407–5410; *Angew. Chem. Int. Ed.* **2008**, *47*, 5327–5330.
[23] G. R. Millward, S. Ramdas, J. M. Thomas, M. T. Barlow, *J. Chem. Soc. Faraday Trans. 2* **1983**, *79*, 1075–1082.
[24] J. M. Thomas, G. R. Millward, D. White, S. Ramdas, *J. Chem. Soc. Chem. Commun.* **1988**, 434–436.
[25] G. Perego, M. Cesari, G. Allegra, *J. Appl. Crystallogr.* **1984**, *17*, 403–410.
[26] G. Kokotailo, US Patent 4229424, **1980**.
[27] http://www.iza-structure.org/databases.
[28] G. González, W. Stracke, Z. Lopez, U. Keller, A. Ricker, R. Reichelt, *Microsc. Microanal.* **2004**, *10*, 224–235.
[29] A. Tuel, Y. B. Taârit, *Zeolites* **1994**, *14*, 169–176.
[30] K. Foger, J. V. Sanders, D. Seddon, *Zeolites* **1984**, *4*, 337–345.
[31] J. P. Arhancet and M. E. Davis, *Chem. Mater.* **1991**, *3*, 567–569.
[32] M. W. Anderson, K. S. Pachis, F. Prébin, S. W. Carr, O. Terasaki, T. Ohsuna, V. Alfreddson, *J. Chem. Soc. Chem. Commun.* **1991**, 1660–1664.
[33] G. González, C. S. González, W. Stracke, R. Reichelt, L. García, *Microporous Mesoporous Mater.* **2007**, 101, 30–42.
[34] E. J. P. Feijen, K. De Vadder, M. H. Bosschaerts, J. L. Lievens, J. A. Martens, P. J. Crobet, P. A. Jacobs, *J. Am. Chem. Soc.* **1994**, *116*, 2950–2957.
[35] M. S. Francesconi, Z. E. López, D. Uzcátegui, G. González, J. C. Hernández, A. Uzcátegui, A. Loaiza, F. E. Imbert, *Catal. Today* **2005**, *107–108*, 809–815.
[36] J. M. Thomas, G. R. Millward, S. Ramdas, M. Audier, *Acta. Chem. Scan.* **1983**, 6, 181–197.
[37] O. Terasaki, J. M. Thomas, G. R. Millward, D. Watanabe, *Chem. Mater.* **1989**, *1*, 158–162.
[38] T. Ohsuna, O. Terasaki, Y. Nakagawa, S. I. Zones, K. Hiraga, *J. Phys. Chem. B* **1997**, *101*, 9881–9885.
[39] J. M. Thomas, G. R. Millward, *J. Chem. Soc. Chem. Commun.* **1982**, 1380–1383.
[40] M. M. J. Treacy, D. E. W. Vaughan, K. G. Strauhmaier, J. M. Newsam, *Proc. R. Soc. London Ser. A* **1996**, *452*, 813–840.
[41] T. Ohsuna, O. Terasaki, V. Alfredsson, J. O. Bovin, D. Watanabe, S. W. Carr, M. W. Anderson, *Proc. R. Soc. London Ser. A* **1996**, *452*, 715–740.
[42] D. M. Bibby, N. B. Milestone, L. P. Aldridge, *Nature* **1979**, *280*, 664–665.
[43] Y. Nakagawa, WO Patent 95/09812, **1995**.
[44] S. I. Zones, A. W. Burton, G. S. Lee, M. M. Olmstead, *J. Am. Chem. Soc.* **2007**, *129*, 9066–9079.
[45] J. B. Nagy, Z. Gabelica, E. G. Derouane, *Zeolites* **1983**, 3, 43–49.
[46] E. de Vos Burchart, H. van Koningsveld, B. van de Graaf, *Microporous Mater.* **1997**, *8*, 215–222.
[47] S. L. Njo, J. H. Koegler, H. van Koningsveld, B. van de Graaf, *Microporous Mater.* **1997**, 8, 223–229.
[48] L. Brabec, M. Kočiřík, *Mater. Chem. Phys.* **2007**, 102, 67–74.
[49] N. M. Ramsahye, B. Slater, *Chem. Commun.* **2006**, 442–444.
[50] J. W. Mullin, *Crystallization*, 4th ed., Butterworth-Heinemann, Oxford, **2001**, pp. 216–288.
[51] S. M. Stevens, K. Jansson, N. S. John, O. Terasaki, M. W. Anderson, M. Castro, P. A. Wright, P. Cubillas in *Studies in Surface Science and Catalysis, Vol. 174* (Eds.: A. Gédéon, P. Massiani, F. Babonneau), Elsevier, Amsterdam, **2008**, pp. 775–780.
[52] N. Hanif, M. W. Anderson, V. Alfredsson, O. Terasaki, *Phys. Chem. Chem. Phys.* **2000**, *2*, 3349–3357.
[53] A. M. Goossens, B. H. Wouters, P. J. Grobet, V. Buschmann, L. Fiermans, J. A. Martens, *Eur. J. Inorg. Chem.* **2001**, 1167–1181.
[54] M. Audier, J. M. Thomas, J. Klinowski, D. A. Jefferson, L. A. Bursill, *J. Phys. Chem.* **1982**, *86*, 581–584.

Received: August 28, 2009
Published online: January 11, 2010

  